EFFECT OF LOCAL WALL THINNING ON FRACTURE BEHAVIOR OF STRAIGHT PIPE

Masato Ono, Ki-Woo Nam*, Koji Takahashi, Kotoji Ando
Department of Safety & Energy Engineering, Yokohama National University
79-5 Tokiwadai, Hodogaya-ku, Yokohama, 240-8501, Japan
Fax: 81-45-339-4024, e-mail: d03ga405@ynu.ac.jp (Masato Ono)
*Pukyong National University, 100 Yongdang-dong, Nam-gu, Busan, 608-080, Korea

Abstract

Effects of circumferentially local wall thinning on the fracture behavior of pipes were investigated by monotonic four-point bending. Local wall thinning was machined on the pipes in order to simulate erosion/corrosion metal loss. The configurations of the eroded area included an eroded ratio of d/t = 0.2, 0.5, 0.6, and 0.8, and an eroded length of l = 10 mm, 25 mm, and 120 mm. Fracture type could be classified into ovalization, local buckling, and crack initiation depending on the eroded length and eroded ratio. Three-dimensional elasto-plastic analyses were also carried out using the finite element method, which is able to accurately simulate fracture behaviors excepting failure due to cracking. It was possible to predict the crack initiation point by estimating true fracture ductility under multi-axial stress conditions at the center of the eroded area.

Introduction

High energy carbon steel pipes are used extensively in piping systems of power plants. For the service periods, high temperature and high pressure water and steam flow at high velocity through these piping systems. Sometimes, theses pipes are subjected to a thinning of the wall thickness at the inside wall due to erosion/corrosion. Therefore, it is important to evaluate the strength and fracture behaviors of the pipes undergoing local wall thinning to maintain the integrity of the piping systems. Researchers have conducted several experiments on carbon steel pipes with local wall thinning in order to evaluate plastic collapse behavior and strength. For example, the fracture behavior of straight, elbow [1], and tee pipes [2] were investigated.

This study was performed to evaluate by experiment the fracture behavior and fracture strength of carbon steel pipes with circumferentially local wall thinning under monotonic load. In addition, the fracture behavior and fracture strength of these pipes were calculated by elasto-plastic analysis using finite element (FE) code ANSYS. We compared the simulated results by finite element analysis with the experimental ones. Moreover, crack initiation point was predicted from equivalent strain and true fracture ductility under multi-axial stress conditions at the center of the eroded area.

Pipe specimens and experimental procedure

The pipe specimens used in the experiments are carbon steel pipes for high pressure service, called ‘STS370’ in JIS (Japanese Industrial Standards), which are commonly used in piping systems of nuclear power plants in Japan. The carbon steel of STS370 is similar to that of ASME A333 Gr.6.

Full-scale experiments were performed on 48.6 mm diameter Schedule 80 STS370 carbon steel straight pipes with circumferentially local wall thinning. In reality, the wall thinning occurs inside the pipes. The fracture behaviors of pipes with wall thinning on the outside of the pipes are almost identical to those of pipes with wall thinning on the inside surface [3]. Thus, the circumferentially local wall thinning was machined on the outside of straight pipes. The boundary between the sound part and the thinned part was rounded to prevent stress concentration. Straight pipe specimens are shown in Fig. 1. A monotonic bending load was applied to straight pipe specimens by four-point bending at room temperature without internal pressure. The major and minor spans of the four-point loading were 600 mm and 150 mm, respectively. Tests were carried out under displacement control of the cross head-speed at 2 mm/min. The eroded depth, *d*, indicates the depth of metal loss in the thickness direction, and the eroded length, *l*, indicates the axial length of the local wall thinning. The ratio of the eroded depth (*d*) to the wall thickness (*t*) of the pipes (eroded ratio) was *d/t*. Table 1 shows the shape and dimensions of specimen.

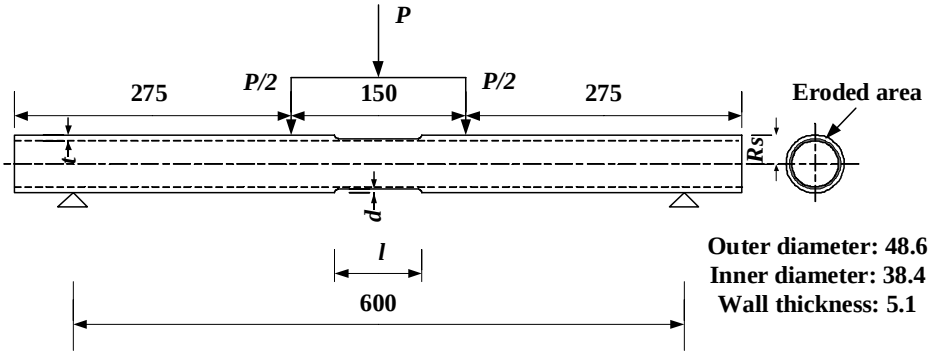

FIGURE 1 Shape and dimensions of a pipe specimen
with circumferentially local wall thinning; dimensions shown in mm.

TABLE 1 Specimen geometries, experimental results, and FE analyses results.

Specimen No.	Eroded ratio (*d/t*)	Eroded length (*l*) / mm	Failure mode	Crack initiation point (δ_c)/ mm	
				Experimen	estimated
WTP-1			Ovalization		
WTP-2	0.8	10	Crack initiation	11	6
WTP-3		25	Buckling		
WTP-4		120			
WTP-5	0.6	10	Crack initiation	13	8
WTP-6	0.5			20	10
WTP-7	0.2		Ovalization		

Finite element analysis

Figures 2(a) and (b) show an example of the FE model. In FE analyses, the elasto-plastic analyses were performed by FE code ANSYS ver. 6.1. Modelled pipes were meshed using a hexahedral element with 20 nodes. The symmetry condition was exploited such that only one quarter of the half space was meshed. In the analyses, von Mises yield criterion was used. The analyses were carried out with the displacement control without internal pressure. The solid line in Fig. 3 shows the relationship between true stress and true strain used for FE analysis. The Young's modulus was 206 GPa, and the Poisson's ratio was 0.3.

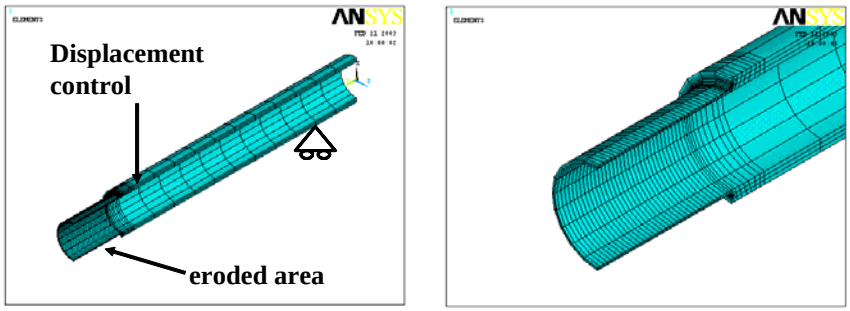

(a) (b)

FIGURE 2 An example of the FE analysis model; (a) 1/4 modeling, (b) detail of thinning area.

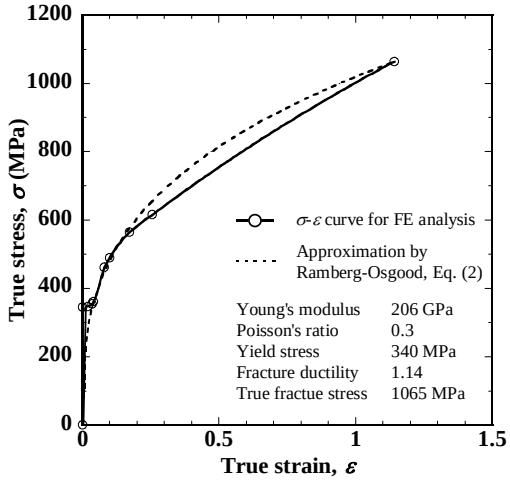

FIGURE 3 Stress-strain curve for FE analysis.

Results and Discussion

1. Experimental results

Failure modes obtained from experiments are summarized in Table 1. In this study, the failure modes were classified into three types: ovalization, local buckling, and crack initiation depending on eroded depth and length.

Figures 4(a) and (b) show typical moment-displacement curves for straight pipe specimens obtained from experiments.

Figure 4(a) shows bending moment-displacement curves for the pipes with the eroded ratio d/t = 0.8. WTP-1 (a pipe with no wall thinning) failed due to ovalization. WTP-2 with l = 10 mm failed due to cracking, and the moment decreased rapidly after the crack initiation and propagation. The crack initiated at the center of the tension side. However, WTP-3 and -4, with l = 25 and 120 mm, respectively, failed due to buckling. The moment was increased a little after the buckling, and the applied moment decreased gradually after the maximum moment. Thus, the WTP-3 and -4 showed sufficient ductility. Buckling occurred at the center of the compression side. The morphology of buckling could be successfully simulated.

Figure 4(b) shows bending moment-displacement curves for the pipe with the eroded length l = 10 mm. WTP-7 with d/t = 0.2 failed due to ovalization. However, WTP-5 and -6,

with d/t = 0.6 and 0.5, respectively, failed due to cracking, and the moment decreased rapidly after crack initiation and propagation. Crack initiated at the center of the tension side.

The eroded ratio affected the failure behavior of the pipe as expected. Moreover, the length also affected the failure behavior, as shown in Fig. 4(a). It is important to note that the pipe with a relatively short eroded length failed due to cracking. An explanation for this is discussed in the following sections.

2. FE analyses

Figures 5 (a) and (b) show bending moment-load point displacement curves obtained from FE analyses for pipes with the eroded ratio d/t = 0.8 and the eroded length l =10 mm, respectively. The results obtained from FE analyses agreed well with the experimental ones except in the cases of WTP-2, -5, and -6. In the experiments of WTP-2, -5, and -6 shown in Fig. 4, the bending moment decreased rapidly due to cracking at the center of the tensile side. In the analysis, in contrast, the crack did not initiate and the bending moment did not decrease.

When the pipes failed by cracking, the fracture behavior could not be successfully predicted by the FE analysis. Thus, we predicted crack initiation by using the estimation method proposed by Miyazaki et al. [4].

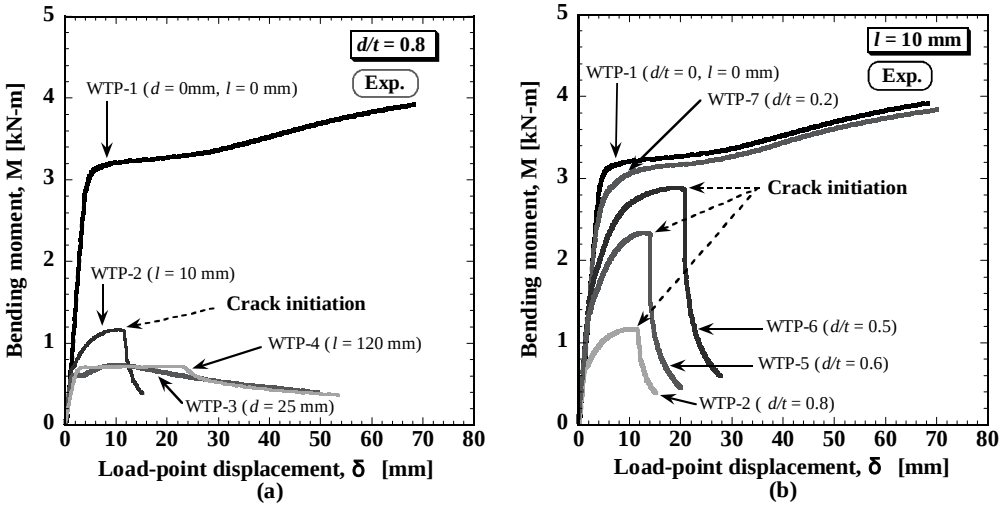

FIGURE 4 Relationship between moment and displacement [Experimental results]

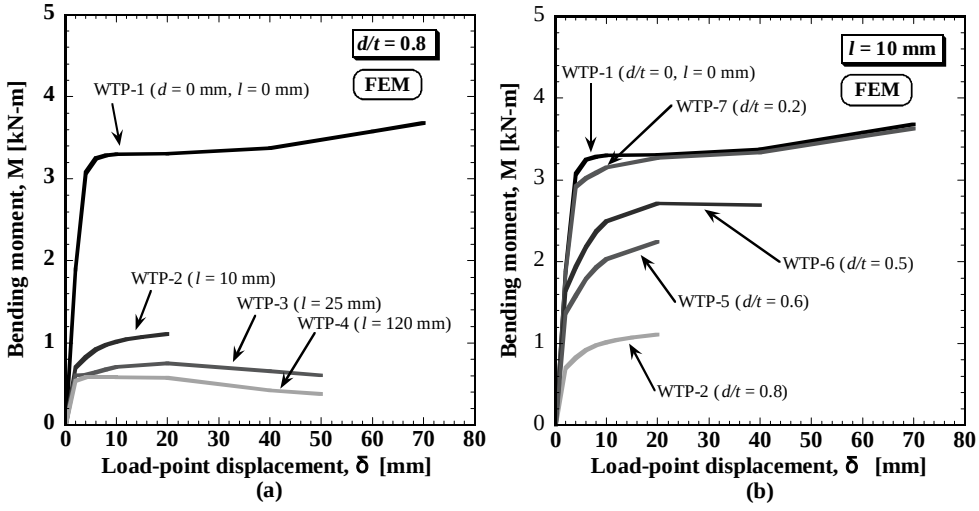

FIGURE 5 Relationship between moment and displacement [Finite element analyses]

3. Prediction of crack initiation at the center of [the] eroded area

Miyazaki et al. extended Weiss's theory [5] to assess true fracture ductility under the multi-axial stress conditions (ε_{mf}) expressed by Eq. (1),

$$\varepsilon_{mf} = \frac{\left(\frac{\omega m \sigma_{uf}}{\sigma_0}\right) + \lambda\left(\frac{\omega m \sigma_{uf}}{\sigma_0}\right)^n}{\left(\frac{\sigma_{uf}}{\sigma_0}\right) + \lambda\left(\frac{\sigma_{uf}}{\sigma_0}\right)^n}\varepsilon_{uf} \qquad (1)$$

$$m = \sqrt{(1+\alpha+\beta)^2 - 3(\alpha+\beta+\alpha\beta)}$$

$$\omega = \frac{1}{1+\alpha+\beta} \quad ,$$

$$\alpha = \sigma_2/\sigma_1, \quad \beta = \sigma_3/\sigma_1$$

where σ_1, σ_2 and σ_3 are principal stresses. The yield stress, σ_0, is 340 MPa. σ_{uf} and ε_{uf} are true fracture stress and true fracture ductility under uniaxial conditions, respectively. The values of σ_{uf} and ε_{uf} are 1065 MPa and 1.14, respectively. λ and n are material constants defined below.

In this estimation, the relationship between true stress and true strain in the wide true strain range up to true fracture ductility (ε_{uf}) was approximated by Ramberg-Osgood equation [6],

$$\left(\frac{\varepsilon_{ms}}{\sigma_0/E}\right) = \left(\frac{\sigma_{ms}}{\sigma_0}\right) + \lambda\left(\frac{\sigma_{ms}}{\sigma_0}\right)^n \quad , \qquad (2)$$

where σ_{ms} and σ_0 are equivalent stress and yield stress, and E and σ_0 are 206 GPa and 340 MPa, respectively. The broken line in Fig. 3 shows the relationship between true stress and true strain approximated by the Ramberg-Osgood equation. The values of λ and n in Eqs. (1) and (2) are 20.4 and 3.11, respectively. The degree of multi-axial stress depends on deformation of the pipes. Thus, the true fracture ductility (ε_{mf}) at the center of the eroded area also depends on deformation. Moreover, equivalent strain (ε_{ms}) increases with deformation of the pipes. It is postulated that crack initiates at the point where equivalent strain (ε_{ms}) exceeds true fracture ductility (ε_{mf}).

In this study, the values of ε_{mf} were estimated by substituting the principal stresses at the center of the eroded area obtained from FE analyses into Eq. (1). The values of ε_{ms} were obtained from the FE analyses.

Crack initiation points (δ_c), the load point displacement where cracks initiated, were estimated by the above method. Table 1 shows crack initiation points (δ_c) obtained from both experiments and estimations.

Figures 6(a) and (b) show the equivalent strain (ε_{ms}) and fracture ductility (ε_{mf}) calculated by Eq. (1) as a function of load point displacement (δ) for WTP-2 and WTP-3, respectively. The broken line and the solid line in Fig. 6 and Fig. 7 show fracture ductility and equivalent strain, respectively. The WTP-2 and WTP-3 failed due to cracking and buckling, respectively. In the experiment, the WTP-3 failed due to buckling and no crack initiated. The fracture ductility and the equivalent strain do not cross in Fig. 6(b), indicating no crack

initiation. In the experiment, therefore, the result of estimation was consistent with that of the experiment. In Fig. 6(a), the fracture ductility and equivalent strain cross at δ_c = 6 mm. Thus, it can be estimated that crack initiated at this point. In the experiment, the crack initiated at δ_c = 11 mm.

The value of ε_{mf} for WTP-2 (l = 10 mm) is lower than that of WTP-3 (l = 25 mm). Moreover, the value of ε_{ms} for WTP-2 is higher than that of WTP-3. Thus, as the eroded length (l) shortens, the specimen tends to fail by cracking. This is because multi-axiality at the eroded area increases due to stress constraint.

Figures 7(a) and (b) show similar results for WTP-6 and WTP-7 with an eroded length of 10 mm. In the experiment, WTP-7 failed due to ovalization. The fracture ductility and the equivalent strain do not cross in Fig. 7 (b), indicating no crack initiation. In the experiment, WTP-6 failed due to cracking. The fracture ductility and equivalent strain cross at δ_c = 10 mm. In the experiment, the crack initiated at δ_c = 20 mm.

Thus, it is possible to estimate the crack initiation point by using true fracture ductility expressed by Eq. (1) and equivalent strain.

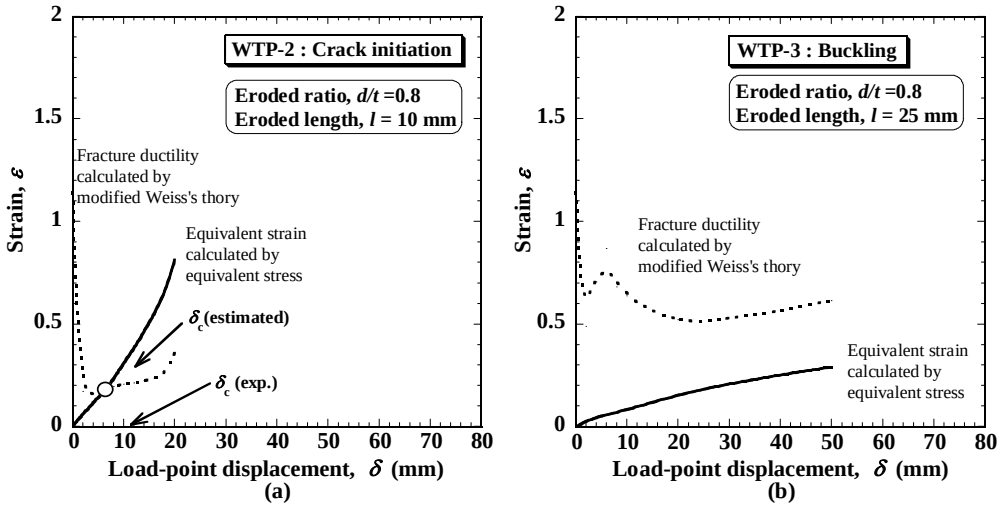

FIGURE 6 Relationship between strain, fracture ductility, and displacement; an example of (a) WTP-2: crack initiation, (b) WTP-3: buckling.

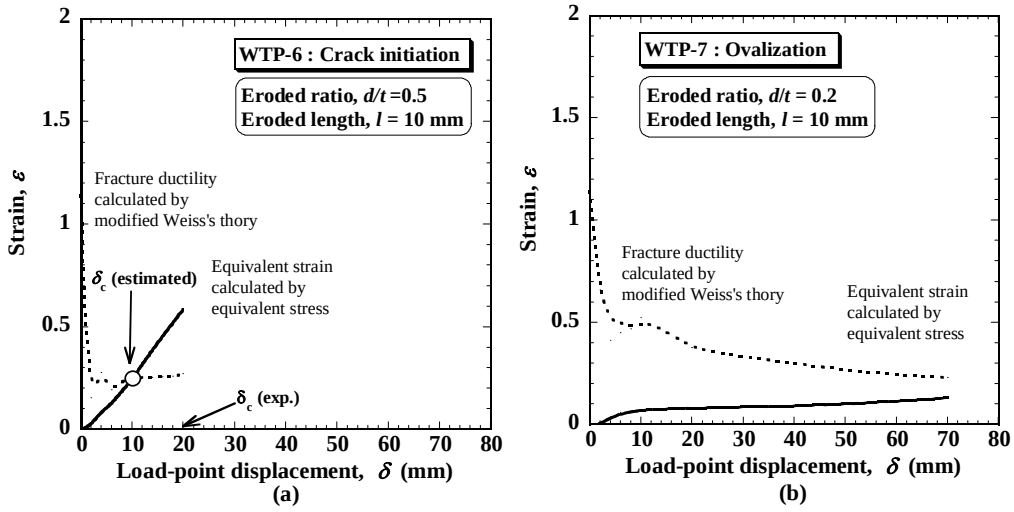

FIGURE 7 Relationship between strain, fracture ductility, and displacement; an example of (a) WTP-6: crack initiation, (b) WTP-7: ovalization.

Conclusion

Fracture behaviors of straight pipes with circumferentially local wall thinning were investigated by monotonic four-point bending tests and FE analyses.

(1) In the case of an eroded ratio (d/t = 0.8), straight pipes with circumferentially local wall thinning with an eroded length (l = 25 and 120 mm) showed sufficient ductility, but those with an eroded length (l = 10 mm) failed due to cracking. Therefore, it should be noted that the pipe with a relatively short eroded length failed due to cracking.

(2) In the case of an eroded length (l = 10 mm), pipe with an eroded ratio (d/t = 0.5 and 0.6) failed due to cracking. Therefore, in the case of a relatively short eroded length, it is important to note that the pipe with even smaller eroded ratio failed due to cracking.

(3) In bending moment-displacement curves, the analytical results agreed well with the experimental ones except in the case of pipe that failed due to cracking.

(4) It is possible to predict crack initiation at the center of the eroded area by using the estimation of true fracture ductility under multi-axial condisions proposed by Miyazaki et al.

References

1. S. H. Ahn, K. W. Nam, Y. S. Yoo, K. Ando, S. H. Ji, M. Ishiwata, K. Hasegawa, *Nuclear Engineering and Design*, 2002, 91
2. K. Takahashi, Y. Kimura, A. Kato, M. Ono, K. Ando, M. Hisatsune, K. Hasegawa, *Journal of High Pressure institute of Japan vol. 41 No. 6*, 2003, 37 (in Japanese)
3. K. Miyazaki, S. Kanno, M. Ishiwata, K. Hasegawa, S. H. Ahn, K. Ando, *Nuclear Engineering and Design*, 1999, 191
4. K. Miyazaki, A. NEBU, S. Kanno, M. Ishiwata, K. Hasegawa, *Journal of High Pressure institute of Japan vol. 40*, 2002, 62 (in Japanese)
5. V. Weiss, *proceeding 1st Int. Conf. on Mechanical Behavior of Materials*, 1972, 159
6. W. Ramberg and W. R. Osgood, *NASA Technical Note*, 1943, 902